International Forum on Aeroelasticity and Structural Dynamics
IFASD 2019
9-13 June 2019, Savannah, Georgia, USA

NUMERICAL AND EXPERIMENTAL STUDY OF AEROELASTIC TAILORING EFFECT USING FLEXIBLE COMPOSITE LAMINATES FOR HAPS APPLICATION

B. Kirsch[1], O. Montagnier[1], T.M. Faure[1], E. Benard[2]

[1]Centre de Recherche de l'Ecole de l'Air (CReA)
Ecole de l'air, B.A. 701, 13661 Salon-Air, France
bertrand.kirsch@ecole-air.fr
olivier.montagnier@ecole-air.fr
thierry.faure@ecole-air.fr

[2]Institut supérieur de l'Aéronautique et de l'Espace
10 Avenue Edouard Belin, 31400 Toulouse, France
emmanuel.benard@isae.fr

Keywords: composite materials, aeroelastic tailoring, high-aspect-ratio wing, wind tunnel test

Abstract: The enhancement of high altitude drone endurance compels to design very flexible high-aspect-ratio composite airframe vulnerable to destructive fluid/structure interaction like flutter or torsional divergence. Extensive research has been conducted to increase critical speed without being at the expense of weight balance, one of the promising solutions is the aeroelastic tailoring which consists in a specific configuration of laminated composite layup. The present work uses an aeroelastic reduced order model, namely GEBTAero, suitable for the non linear anisotropic behavior of this kind of composite wing, able to quickly compute aeroelastic critical speeds. Particular focus is put on a wind tunnel test campaign conducted on a set of flexible plates, both metallic and composite, in order to assess the accuracy of GEBTAero.

1 INTRODUCTION

Recent progress made in the field of solar cells, energy storage and composite materials pave the way to a new concept of aircraft, namely High Altitude Pseudo Satellite (HAPS). Among them, a particular type of solar or/and hydrogen powered High Altitude Long Endurance (HALE) Unmanned Aerial Vehicles (UAV) aims to meet a virtually infinite endurance. To achieve this far-reaching goal, aerodynamic and structural performances are stretched to their limits because of the low on-board power. This results, on the aerodynamic side, in high-aspect ratio wing optimising the lift-to-drag ratio and, on the structural side, in lightweight very flexible composite airframe. The main drawback of this particular design is its vulnerability to destructive fluid/structure interactions like torsional divergence and flutter which are difficult to predict because of the tight coupling between aerodynamics, structure and flight mechanics. Classical solutions designed to further aeroelastic critical speed mostly rely on the stiffening of the airframe or the adjustment of mass distribution. Both options are detrimental to mass balance, which is a key feature of HAPS. In that context, alternative solutions should be explored, among these are aeroelastic tailoring, a technology born in the 1970s with the forward-swept wing experimental plane X-29. It consists in using laminate layup without mirror symmetry or-and unbalanced layup. The emerging structural coupling induced on the aerodynamic side a

coupling between the bending, due to lift forces, and the twisting of the wing which determines the local Angle of Attack (AoA) and consequently an impact on aeroelastic behavior.

The computational cost of high fidelity aeroelastic simulation on Very Flexible Aircraft (VFA) is still prohibitive prompting the need for suitable reduced order model. Many reduced order model tools have been developed during the last decades. We could mention computation code NANSI (Nonlinear-Aerodynamics/ Nonlinear-Structure Interaction) [1] which combines an Unsteady Vortex Lattice Method (UVLM) and a nonlinear beam theory. The UVLM is particularly useful in case of low-aspect-ratio wing or delta wing because the method is able to predict 3D effects. Another solution is proposed by Murua in SHARP program (Simulation of High Aspect Ratio Planes) [2] using UVLM with a displacement based geometrically exact beam theory. Because of the high aspect ratio of VFA wings, a lot of models rely on the coupling between a beam theory on the structural side and an unsteady aerodynamic strip theory on the aerodynamic side. This is the case of ASWING developed by Drela [3] combining a nonlinear isotropic beam formulation with an unsteady lifting line theory. UM/NAST (University of Michigan/ Nonlinear Aeroelastic Simulation Toolbox), developed by Shearer and Cesnik [4] uses a strain-based geometrically nonlinear beam formulation linked with a finite state two-dimensional incompressible flow aerodynamic theory proposed by Peters et al. [5]. A similar formulation is used by Ribeiro in the Matlab toolbox Aeroflex [6]. One last example is the Matlab toolbox NATASHA (Nonlinear Aeroelastic Trim and Stability of HALE Aircraft) [7] which relies on an intrinsic beam formulation coupled with Peters' theory. In the present work, GEBTAero [8,9], developed by the author, extends the structural solver GEBT developed by Yu and Blair [10] and Wang et al. [11] with a tight coupling with Peters theory in an open source implementation dedicated to high aspect ratio composite wing optimisation using aeroelastic tailoring.

Every computation code need to be evaluated against test cases. The most famous aeroelastic test case is probably the Goland wing [12], with the advantage of being widely used is the community but which is not adapted to VFA (flutter speed is high for incompressible hypothesis and the wing is not flexible). More recently, the Patil wing [13] proposes a more suitable test case to asses the impact of geometrical non linearities on aeroelastic behaviour, but still with an isotropic wing. GEBTAero has been tested against this two test cases with a good agreement [14]. On the experimental side, there is only little data available is the literature concerning flexible wing. We could mention the wind tunnel test conducted by Tang and Dowell [15] on a flexible wing made of a steel flat plate with a balsa wing skin. Although this experiment give interesting results, notably in terms of Limit Cycle Oscillation (LCO) studies, the aeroelastic tailoring effect is not taken into account on this isotropic wing.

This paper presents a wind tunnel test campaign conducted on flexible flat plates, both metallic and composites. First, the aeroelastic reduced order model used in GEBTAero is presented. Then, after a short presentation of the experimental setup, the flutter speed and frequency of an aluminium flat plate is evaluated depending on the half-span. Finally, experimental results for laminates with different layups are presented.

2 AEROELASTIC REDUCED ORDER MODEL

The main objective of GEBTAero is to define a fast implementation of a proper reduced order aeroelastic model well fitted for the computationally intensive task of aeroelastic tailoring optimisation. It relies on the use of optimised open source programs and libraries (sparse direct linear solver MUMPS [16], sparse eigenvalues solver ARPACK [17]).

The high-aspect-ratio assumption gives us the opportunity to neglect three-dimensional effects and thus to use a strip theory which can be easily linked to a beam formulation. A tight coupling is chosen, done by integrating aerodynamic loads directly into the weak formulation of the beam theory. It permits the determination of the aeroelastic modes of the wing about a geometrically non linear steady state, namely frequencies, modal shapes and damping factors. The latter is a key parameter for our study because it defines the limit between stable and unstable speed.

On the structural side, to ensure a proper modelling of the laminate anisotropy and geometrical non linearity, the choice fell on an open source tool named GEBT (Geometrically Exact Beam Theory) developed by Yu and Blair [10] and Wang et al. [11] designed for composite slender structures under large deflections and rotations, assuming the strains to be small. This tool coded in Fortran 90/95 implements a mixed variational formulation based on exact intrinsic equations for dynamics of moving beams developed by Hodges [18]. The main strength of this method, compared to classical displacement based formulation, is to avoid the dependency from a coordinate system (intrinsic nature) for the position and rotation parameters. Kinematical and constitutive relations are then added to the weak formulation with Lagrange multipliers (mixed nature). The resulting formulation allow a finite element implementation with very simple shape functions (constant or linear).

Because of the large displacement and rotation of the wing, three different frame are required (figure 1a):

- a unique global body attached frame a $(\vec{x}_a, \vec{y}_a, \vec{z}_a)$ moving with a given linear and angular velocity $\vec{v}_a$ and $\vec{\boldsymbol{\omega}}_a$ in an inertial frame and consistent with flight mechanics conventions ($\vec{x}_a$ pointing upwards, $\vec{y}_a$ pointing the right wing and $\vec{z}_a$ pointing downwards).
- at least one undeformed beam frame b $(\vec{x}_b, \vec{y}_b, \vec{z}_b)$ fixed in frame a: $\vec{x}_b$ is tangent to the reference line of the undeformed beam. In our case, a frame b is defined for each section of the wing with a different dihedral or/and wing-sweep.
- a deformed beam frame B $(\vec{x}_B, \vec{y}_B, \vec{z}_B)$ for each beam element: $\vec{x}_B$ is tangent to the deformed beam reference line and points to the right, $\vec{y}_B$ has a chordwise direction and points the upstream flow and $\vec{z}_B$ completes the triad.

The cross section parameters of the anisotropic beam are determined using an homogenisation tool following a method developed by Cartraud and Messager [19]. It consists in a three-dimensional finite element calculation realized with the open source solver CalculiX [20] on a Representative Volume Element (RVE) of the beam using periodic boundary conditions along beam axis direction [8]. The RVE is a 3D mesh written in Abaqus input format. Different cases are considered:

- simple shape constant cross section (plate or box): the mesh is automatically generated using the pre/postprocessor CalculiX GraphiX;
- constant cross section: a 2D mesh is extruded with a unique element spanwise;
- periodic cross section: a wing section representing a beam period is meshed (between two ribs for instance).

On the aerodynamic side , the unsteady two-dimensional finite state approximation model developed by Peters et al. [5] is used. This formulation is implemented in our toolbox with the following aerodynamic loads:

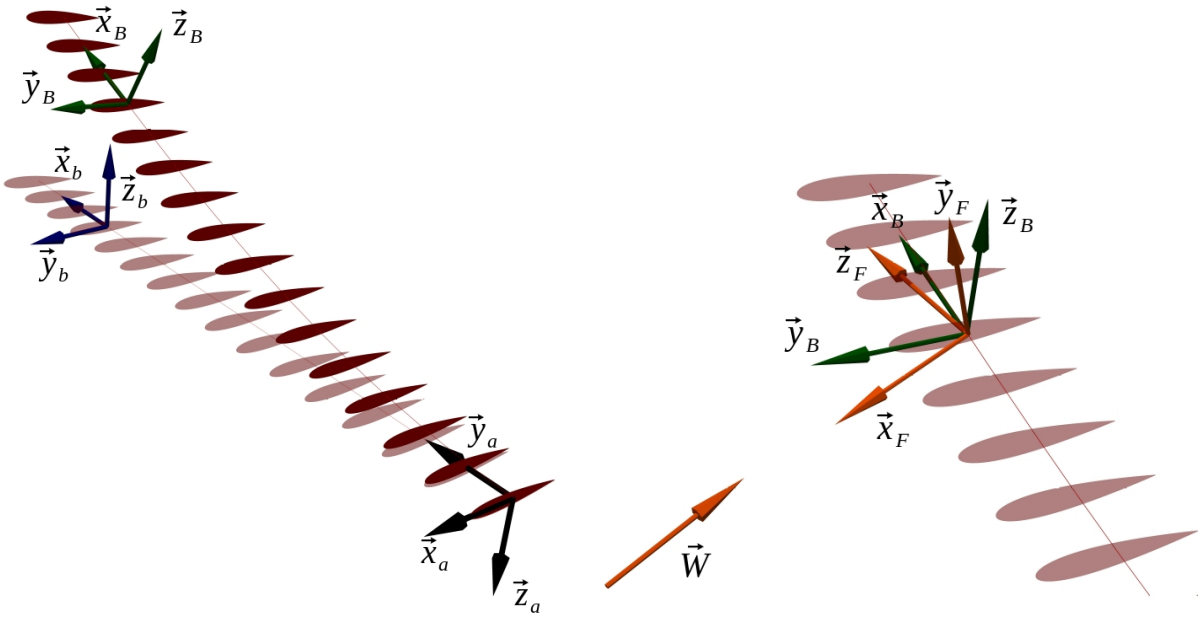

(a) (b)

Figure 1: Frames definition: a) structural frames, b) aerodynamic frame.

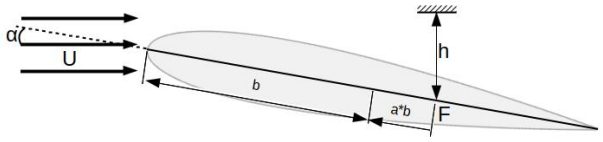

Figure 2: Airfoil parameters

$$L = \pi\rho b^2 \left(\ddot{h} + U\dot{\alpha} - ba\ddot{\alpha}\right) + 2\pi\rho Ub \left[\dot{h} + U\alpha + b\left(\frac{1}{2} - a\right)\dot{\alpha} - \lambda_0\right] \tag{1}$$

$$M = b\left(\frac{1}{2} + a\right) L - \pi\rho b^3 \left[\frac{1}{2}\ddot{h} + u\dot{\alpha} + b\left(\frac{1}{8} - \frac{a}{2}\right)\ddot{\alpha}\right] \tag{2}$$

with L the linear lift, M the linear moment around a reference point F, ρ the air density and U the flow velocity. The semi-chord b, the height h, AoA α and the distance a between the point F and the semi-chord are detailed in Fig. 2.

The induced-flow velocity λ_0 is approximated using N_S induced-flow states $\lambda_1, \lambda_2, \ldots, \lambda_{N_S}$ by:

$$\lambda_0 \approx \frac{1}{2}\sum_{n=1}^{N_S} b_n \lambda_n$$

where the b_n are found in [21] by the least-square method. The λ_n are determined using a set of N_S first-order ODEs as detailled in [21]. The aerodynamic model adds N_S equations for each beam element, the coupled aeroelastic system contains $(18 + N_S)\, N + 12$ equations and the same number of unknowns with N the number of beam elements, providing that structural unknowns are completed with $N \times N_S$ induced-flow states λ_{n_i}.

The tight coupling between structural and aerodynamic models is done using a forth frame F $(\vec{x}_F, \vec{y}_F, \vec{z}_F)$ defined in figure 1b. The resulting formulation permits different applications

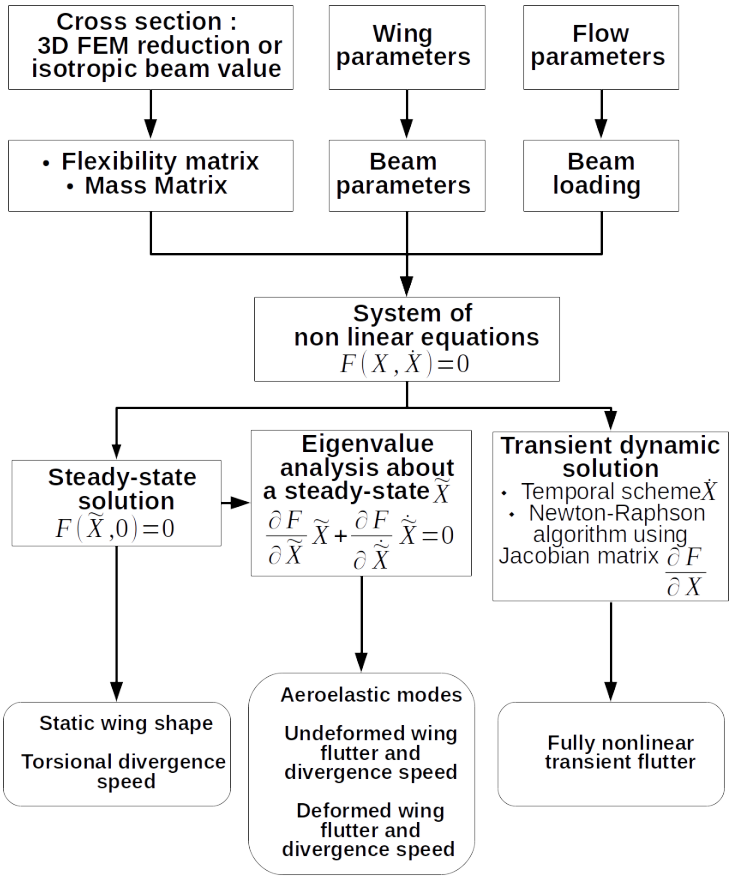

Figure 3: GEBTAero computation features

both in time domain and frequency domain. The capabilities of the resulting program called "GEBTAero" are summarize in figure 3. A particular aspect of this computation code is its capability to quickly compute critical speeds, thanks notably to a modal resolution strategy based on the computation of only a few modes of interest using Arpack modal solver, and the use of sparse matrix [9].

3 EXPERIMENTAL RESULTS

3.1 Experimental setup

The experimental campaign is conducted in a wind tunnel with a test section of $450 \times 450 \times 650$ mm and a speed range from 5 to 45 m/s. The flat plate is mounted using a 3D printed device linked to the side wall of the wind tunnel. The AoA is adjustable using a rotating disk mounted on an axis (figure 4). Thereafter, all the tests are done with an AoA set to zero. The mean flow speed is measured using a differential pressure sensor between the inlet and the outlet of the convergent placed before the test section. In order to evaluate the accuracy of flutter speeds computed by GEBTAero, this experiments focuses on the flutter boundary without the need of studying LCO. In this regard, flat plates could be a good choice. Indeed, provided that the relative thickness is small enough to avoid the need for a milled leading edge and trailing edge, flat plates are good candidates for test cases because of their simplicity. The elastic, inertial and geometrical parameters are easy to determine and the shape is adapted to aerodynamic model as long as the angle of attack remains small. Both metallic and composites plates are tested because of their complementarity. All the parameters are well known for the first one, especially the thickness, which is a very sensitive parameter regarding the aeroelastic behaviour. Different values of bending/twisting coupling coefficient can be set set for the second one.

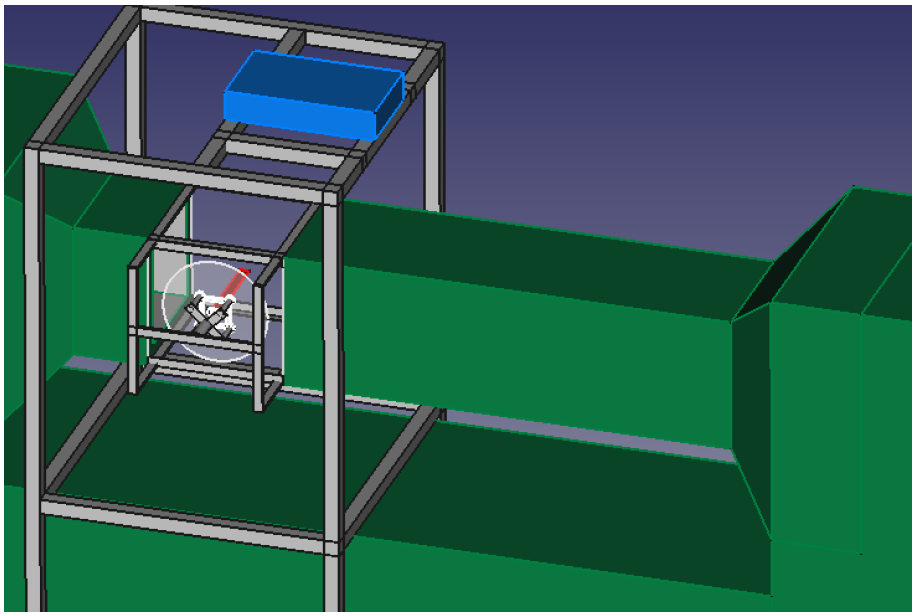

Figure 4: Overview of the experimental set-up

Concerning the measures, the large displacement and rotation of the plate, the flexibility and the small weight of such a plate make it difficult to choose a proper type of sensors to assess flutter speed and frequency. To tackle those constraints, two micro-accelerometers are used (B&K DeltaTron type 4517 ($0,65\,\mathrm{g}$, $8,15 \times 6,35 \times 3,8\,\mathrm{mm}$, bandwidth $1\,\mathrm{Hz}$ to $20\,\mathrm{kHz}$). They are little intrusive and allow to retrieve speed and displacement data throw the integration of the signal.

3.2 Flexible metallic plates

First of all, material and dimensions are set according to the desired aeroelastic performance. The static deflection of the plate, submitted to its own weight, only depends on the Young modulus E, the material density ρ_s, the plate half-span l and the thickness h in accordance with equation 3:

$$f = \frac{3}{2}\frac{\rho_s g l^4}{E h^2} \tag{3}$$

with f the static deflection of the wing tip. Two materials are tested (ν is the Poisson coefficient):

- a steel ($E = 225\,\mathrm{GPa}$, $\nu = 0,3$, $\rho_s = 8640\,\mathrm{kg.m^{-3}}$); available thickness: $0,5\,\mathrm{mm}$ and $0,75\,\mathrm{mm}$;
- an aluminium alloy ($E = 64\,\mathrm{GPa}$, $\nu = 0,33$, $\rho_s = 3000\,\mathrm{kg.m^{-3}}$); available thickness: $0,5\,\mathrm{mm}$ and $0,8\,\mathrm{mm}$.

Static deflection for the maximal half-span of $450\,\mathrm{mm}$ are computed with GEBTAero for the different materials and thickness (table 1). A thickness of $0.5\,\mathrm{mm}$ seems to be a good choice, the relative static deflection of steel and aluminium plates are of the order of the Patil wing test case ($18.25\,\%$). To choose the chord and the material of the plate, a simulation is conducted with GEBTAero with gravity effect (figure 5). First, the analytical value of the divergence speed of

Table 1: Wing tip displacement depending on the thickness and the material for a half-span of $450\,\mathrm{mm}$.

material	thickness	static deflection	
	mm	mm	%
steel	$0,5$	$89,72$	$19,7$
	$0,75$	$40,92$	$9,1$
aluminium	$0,5$	$107,9$	$24,0$
	$0,8$	$33,9$	$9,8$

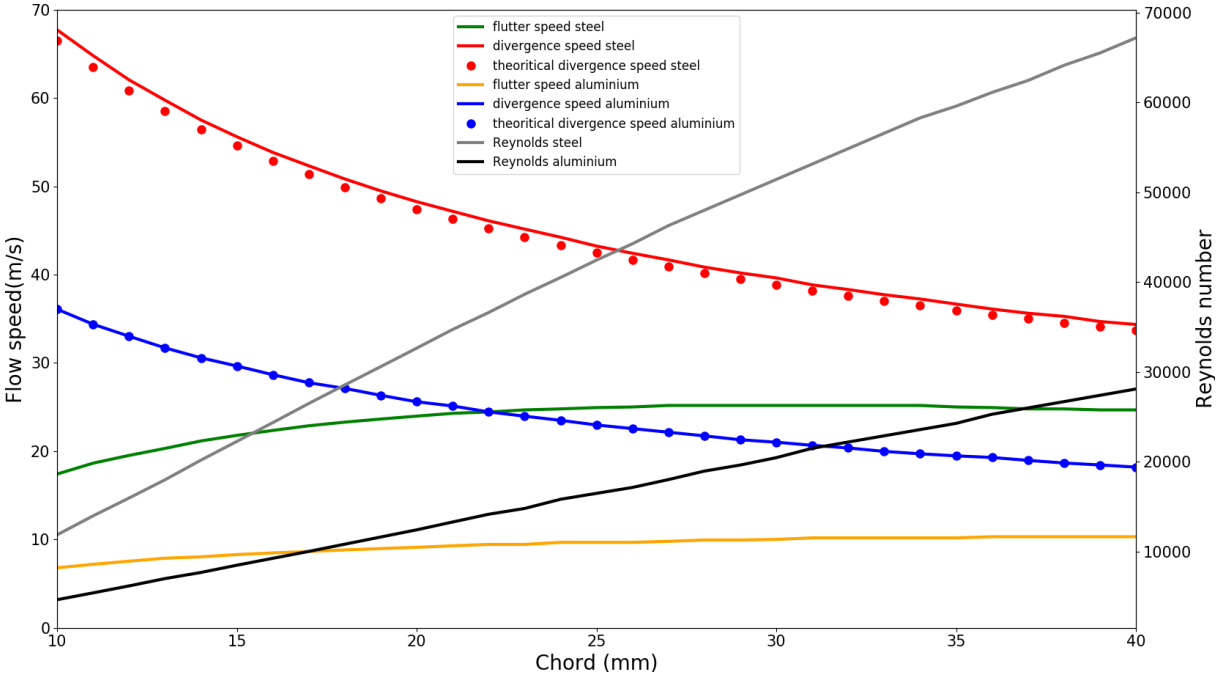

Figure 5: Critical speed and Reynolds number depending on chord for a half-span of $450\,\mathrm{mm}$.

an undeformed flat plate [22], using equation 4, is compared to the one given by GEBTAero :

$$U_{div} = \frac{2\pi}{l}\sqrt{\frac{2GJ}{\rho_s c^2 C_{l,\alpha}}} \tag{4}$$

with $G = E/\left[2\left(1+\nu\right)\right]$ the Coulomb modulus, J the torsion constant and $C_{l,\alpha}$ the lift coefficient slope. $C_{l,\alpha}$ is set to 2π in accordance with the aerodynamic model used (equation 1), J is determined using the equation 5 [23]:

$$J = ch^3\left[\frac{1}{3} - 3.36\frac{h}{16c}\left(1 - \frac{h^4}{12c^4}\right)\right] \tag{5}$$

with c the plate chord, assuming that $h \ll c$.

We can see a very good agreement, all the more since the slight discrepancy for the steel plate vanish for a simulation without gravity effect. In term of flutter speed, the high value for steel plate implies a severe instability with a risk a breaking during the test, considering that flutter speed will be higher for shorter half-span. Then the choice fell on the aluminium plate, with a chord of $30\,\mathrm{mm}$, ensuring a compromise between the Reynolds number and the aspect ratio. The micro-acceleromters are glued on the plate using cyanoacrylate according to figure 6. They

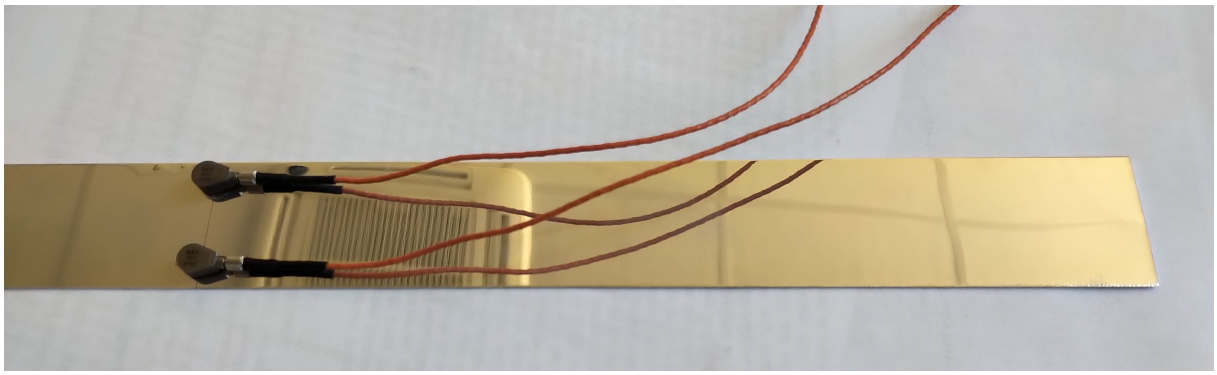

Figure 6: Micro-accelerometers set-up on the flexible aluminium plate.

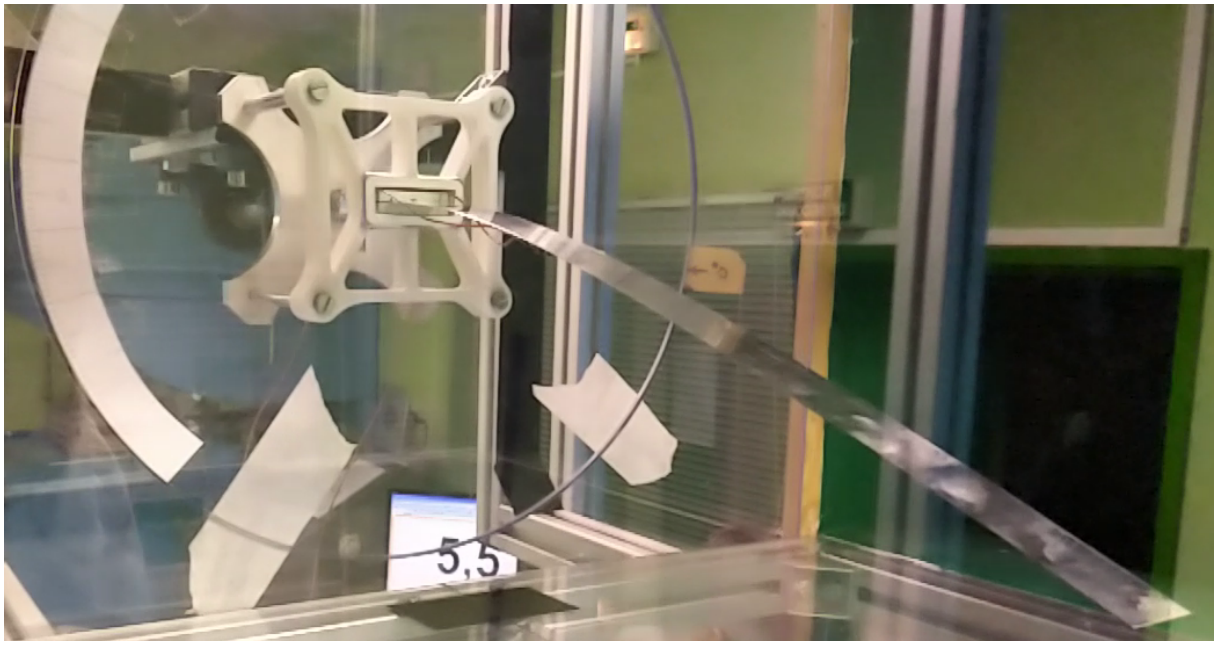

Figure 7: Metallic plate experimental setup

are positioned side by side at 300 mm from the wing tip in order to obtain the vertical acceleration (mean values of the two signals) and the angular acceleration (difference between the two signals scaled by the lever arm). The global setup is shown in figure 7.

Acceleration Power Spectral Density (PSD) are computed for different constant values of constant flow speed, upward to the instability and then downward. The result, for a half-span of 450 mm is plotted in figure 8. The width of every PSD strip correspond to the speed shift between two measures. The flow speed of every PSD strip is written in its bottom left corner. First of all, we could mention a large flow speed hysteresis: instability starts between 11 and 11.5 m/s and stops below 7 m/s. Then, the order of magnitude difference between stable and unstable domain is large, allowing us to easily set the frontier. We can also see two harmonics typical of a non linear instability. To asses the flutter speed and frequency correlation with numerical simulation in a more general manner, the same experiment is done for various half-span ranging from 380 mm to 450 mm. Flutter instability for half-span smaller than 380 mm is too violent and damages the plate. One measure is made for the fundamental frequency and is compared to the second and third mode simulated by GEBTAero (figure 9). According to the simulation, the unstable mode is the third one (in green) which correspond, without flow, to the first twisting mode. However, the correlation with the second mode (in yellow) which correspond, without

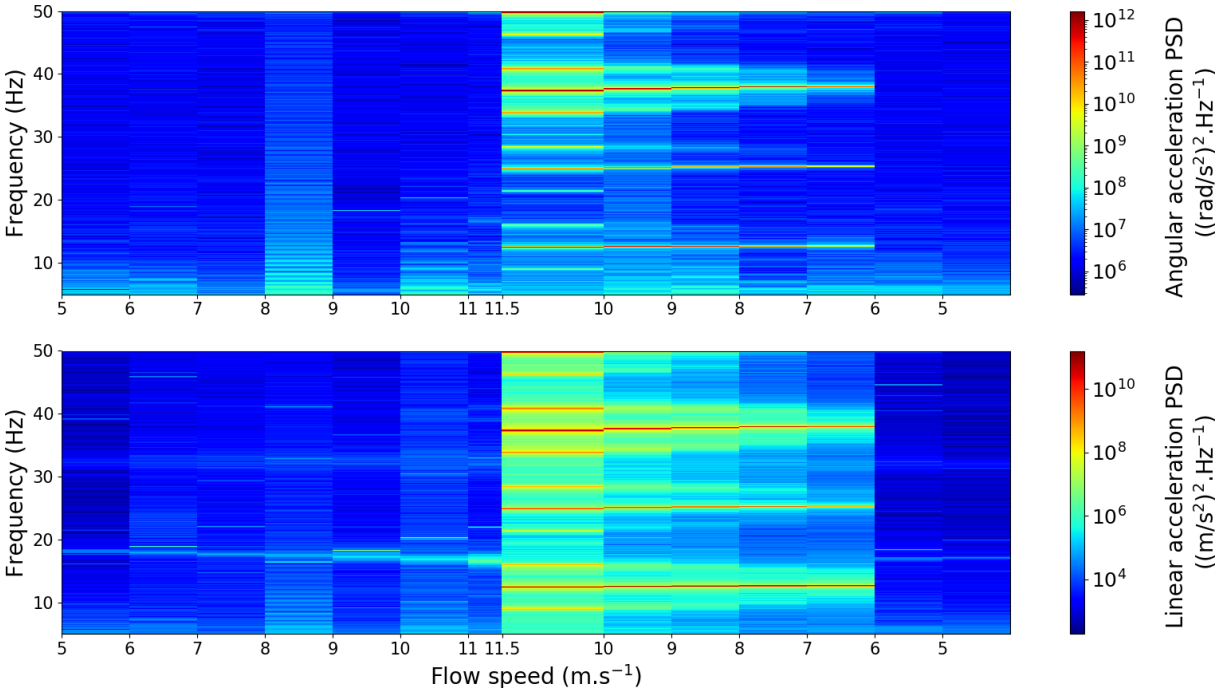

Figure 8: Angular and linear acceleration PSD for an aluminium plate $0.5 \times 30 \times 450$ mm

flow, to the second bending mode, seems to be better.

Concerning the flutter speed, the measurements are made on three different plates with the same dimension to assess repeatability (figure 10). As we can see, the flutter speed is slightly underestimate for the largest values of half-span. It could be an effect of the pressure losses due to the side effect of the wind tunnel. Overall, the agreement between simulation and experiment is quite good. The repeatability is correct, however, especially for largest speed, a very slow bending mode tends to modify the static deflection of the plate, which is a key parameter of the flutter speed.

3.3 Flexible composite plates

In order to evaluate the anisotropic capability of GEBTAero, the same type of experiment is conducted on flexible laminate plates with bending/twisting coupling. The UniDirectional (UD) prepreg used is a UD150/CHS/M10R, its characteristics are presented in table 2. In the same

Table 2: Prepreg HexPly UD150/CHS/M10R characteristics.

	unit	value
mass per unit area	g/m^2	150
nominal cured ply thickness	mm	$0,16$
nominal fiber volume	%	$0,52$
nominal laminate density	g/cm^3	$1,57$
longitudinal Young's modulus E_l (fiber fraction 52%)	Mpa	125
transverse Young's modulus E_t (fiber fraction 52%)	Mpa	$9,3$
Coulomb's modulus G_{lt}	Mpa	$7,75$

way as for metallic plate, simple solutions are seeking to produce relevant test cases. A laminate layup is defined by the orientation of its plies $[\theta_1, \ldots, \theta_n]$. According to the Classical Laminate Theory (CLT), a laminate without mirror symmetry, i.e. without symmetrical plies

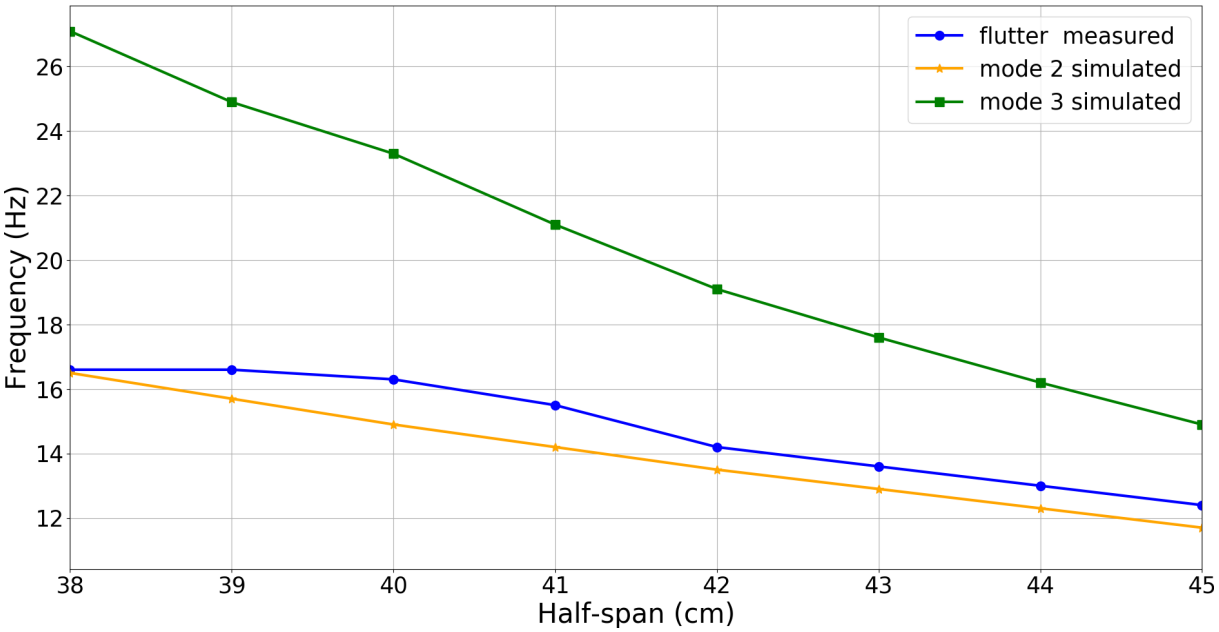

Figure 9: Comparison between experimental and numerical frequencies for a flexible aluminium plate with a section of $0,5\,\mathrm{mm} \times 30\,\mathrm{mm}$ and a variable length.

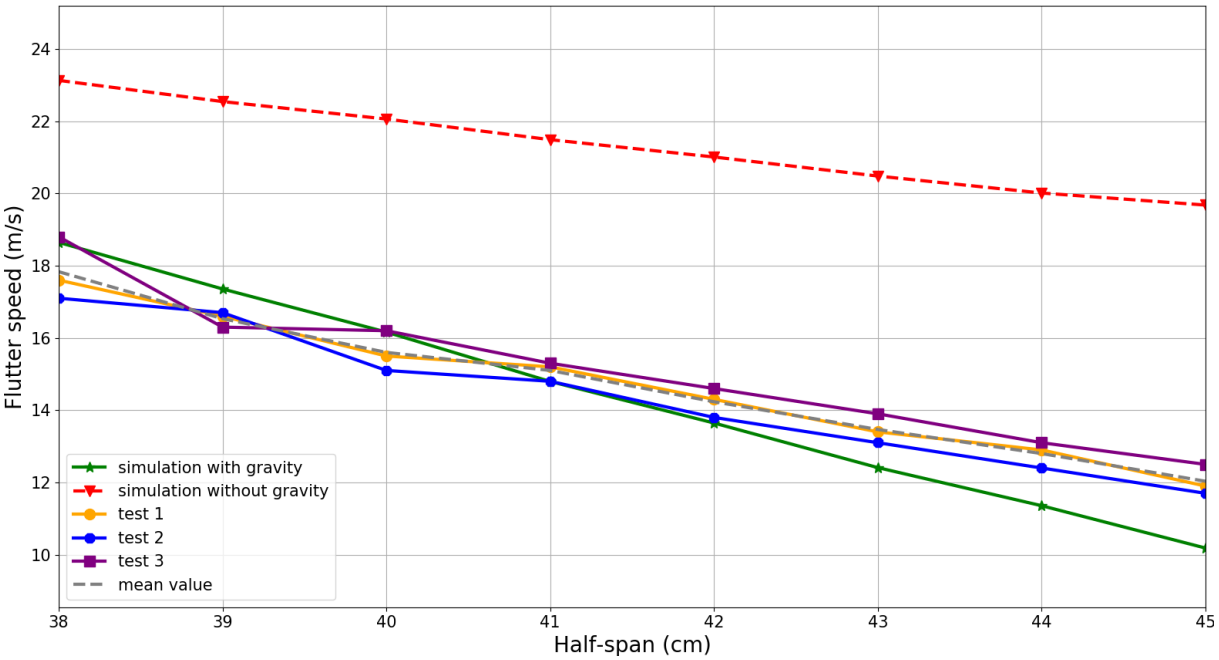

Figure 10: Comparison between experimental and numerical flutter speed for a flexible aluminium plate with a section of $0,5\,\mathrm{mm} \times 30\,\mathrm{mm}$ and a variable length.

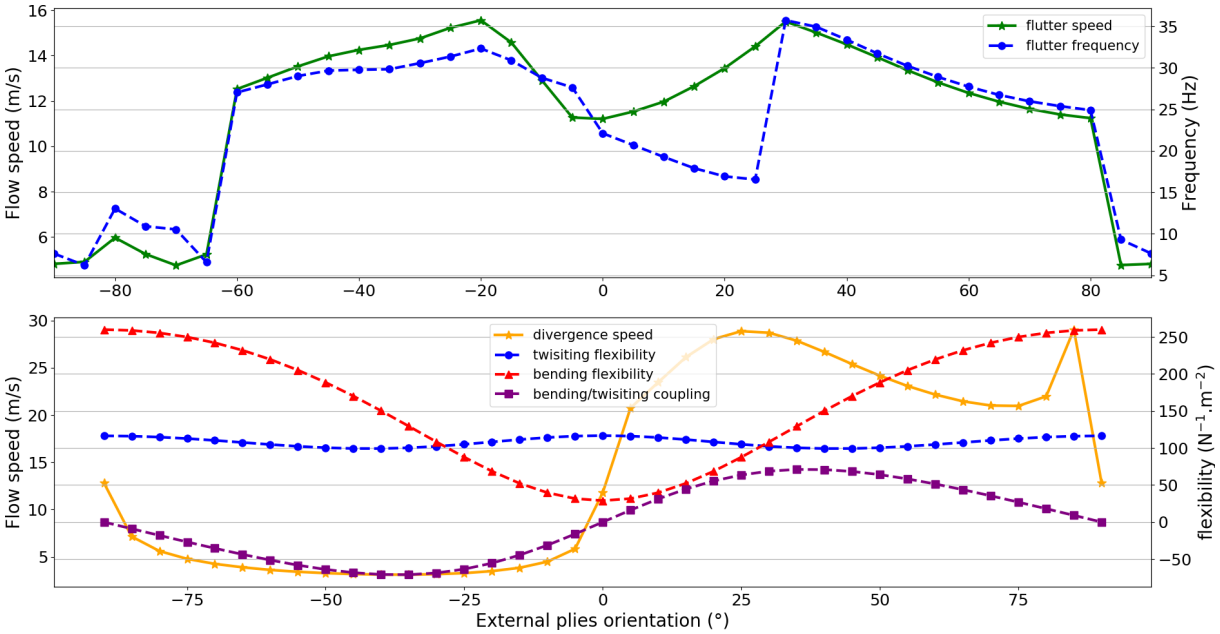

Figure 11: $420\,\mathrm{mm}$ half-span laminate with a central ply oriented at $0°$ and two external plies with various orientation: flutter speed and frequency, divergence speed and flexibility.

to the middle plan with the same orientation, has a traction/twisting coupling. This coupling could be exploited in a wing box configuration, providing that the bending of the wing produce a traction or a compression of the upper side and lower side. Thin plates exploit another type of coupling, generated by unbalanced layup, i.e. without a balance between positive and negative orientation. For example, for a balanced layup, every $45°$ oriented ply is compensated by a $-45°$ ply.

The simplest unbalanced layup consists in a laminate with a single orientation. Although it permits to produce a bending/twisting coupling, such a flexible plate is too fragile and may break between two fibers. The next configuration in terms of complexity is a two-ply laminate with two different fiber orientations. In that case, because mirror symmetry is not respected, the large difference between longitudinal and transverse coefficient of thermal expansion produces an undesired twisting of the plate during the cool down. Then, the simplest usable layup consists in a three-ply laminate with external plies oriented in the same direction. To obtain the proper static deflection and for solidity purposes, the central ply is oriented at $0°$. The divergence and flutter speed, the flutter frequency and the flexibility matrix coefficients simulated by GEBTAero for different external plies orientations are plotted in figure 11. The half-span is set to $420\,\mathrm{mm}$ in order to alleviate wind tunnel test section side effect.

According to the simulation, five layups are produced : $[15, 0, 15]$, $[30, 0, 30]$, $[45, 0, 45]$, $[60, 0, 60]$ and $[90, 0, 90]$, allowing to simulate various aeroelastic behaviour. A sixth one is produced to evaluate another central ply orientation, namely $[30, -30, 30]$. Theoretically, it gives us five more layup by returning the plate ($[15, 0, 15]$ becomes $[-15, 0, -15]$). In fact, negative external plies orientation implies a very low divergence speed with massive stall and is therefore unusable. To illustrate the structural coupling of this laminates, static deflection of plates are shown in figure 12. Beyond the obvious discrepancy in term of bending flexibility, it shows us the structural coupling between the bending due to weight and the twisting of the cross section (except from the uncoupled $[90, 0, 90]$ laminate).

Figure 12: Laminate static deflection, from left to right : $[90, 0, 90]$, $[60, 0, 60]$, $[45, 0, 45]$, $[30, -30, 30]$, $[30, 0, 30]$ and $[15, 0, 15]$.

Contrary to the metallic plate experimental campaign, the flow speed measurement is synchronize with the acceleration measurement, allowing us to produce a spectrogram. During the test, the flow speed is slowly increased until flutter instability and then decreased. The mean flow speed is plotted on the spectrogram. The results for the layups $[15, 0, 15]$ (with coupling) and $[90, 0, 90]$ (without coupling) are plotted in figure 13 and 14, compared to the aeroelastic modes plotted by GEBTAero.

The dynamic behaviour of the $[90, 0, 90]$ laminate plate seems to be similar than metallic plate, with a very low flutter speed thanks to a large flexibility coupled with a low density. However, the $[15, 0, 15]$ laminate plate exhibit a much more complex aeroelastic behaviour, with different type of LCO. To illustrate that complexity, a phase portrait of the vertical dof is proposed, in addition with a long exposure photography, relative to the first instability for an upward flow speed of $9.9\,$m/s (figure 15). This instability concerns mainly the vertical dof, with limited magnitude, suggesting that stall are not involved and thus that this LCO may be caused only by structural non linearities.

Finally, flutter speeds (figure 16) and frequencies (figure 17) are compared to the values simulated by GEBTAero for the five layups with a central ply oriented at $0°$. Regarding frequencies, the first four modes are also plotted. . One the one hand, for the flutter speed, the simulation tends to overestimate the value. However, because the vacuum was not perfectly controlled during the cure process, a discrepancy exist in the laminate thickness (measured from $0.48\,$mm to $0.55\,$mm instead of the nominal $0.48\,$mm), while it is a key parameter in terms of aeroelastic behaviour sensitivity, according to CLT. The other remarkable point is that the bending/twisting coupling tends to compensate the effect of the large deflection due to the gravity in terms of

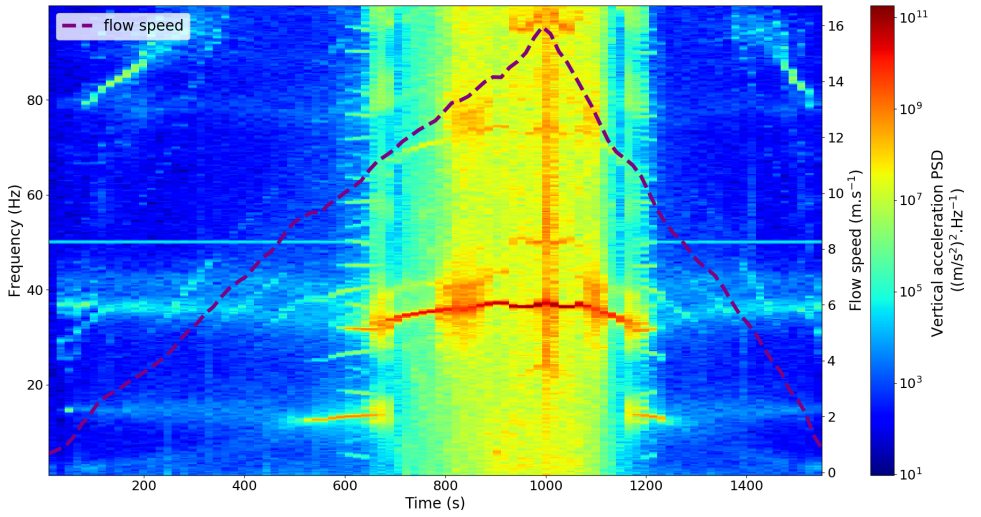

(a)

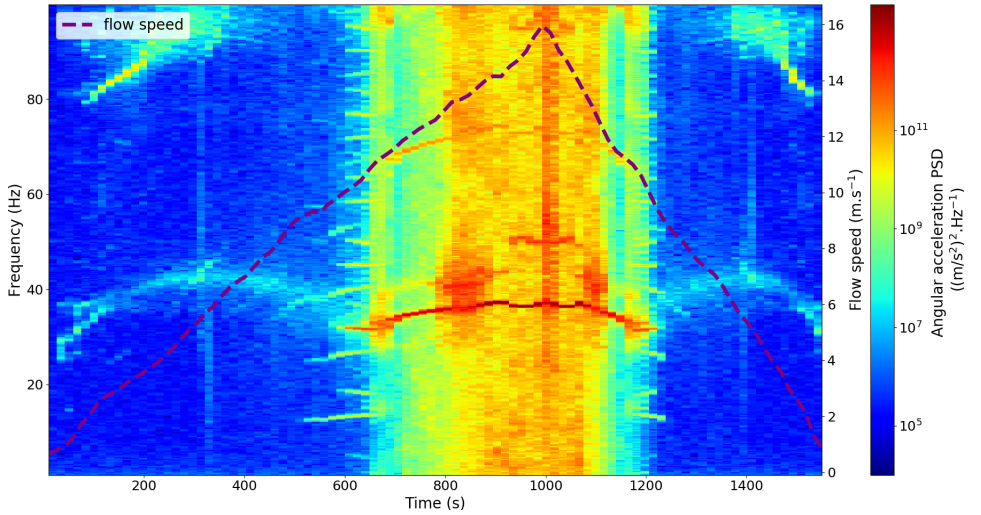

(b)

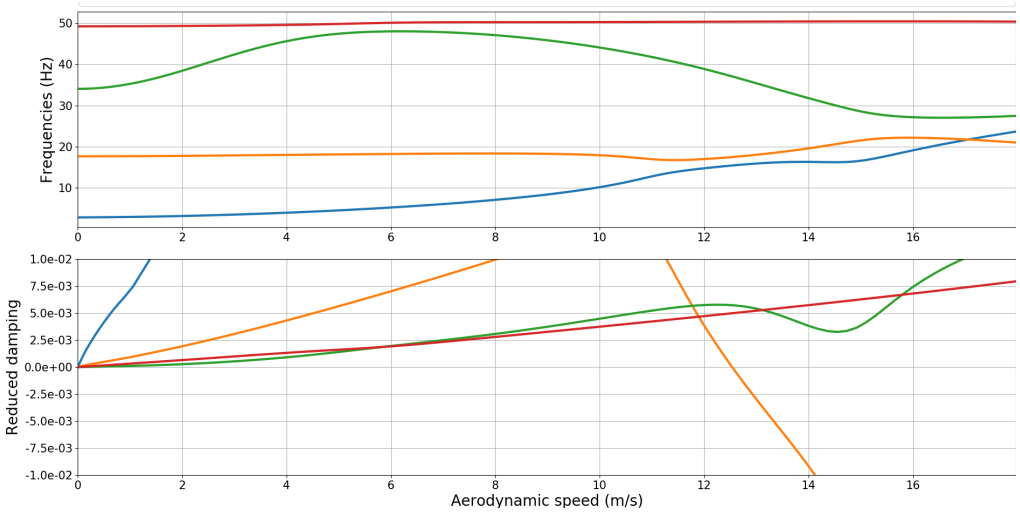

(c)

Figure 13: $420\,\mathrm{mm}$ half-span $[15, 0, 15]$ laminate test result: a) vertical acceleration spectrogram, b) angular acceleration spectrogram, c) GEBTAero aeroelastic modes plot.

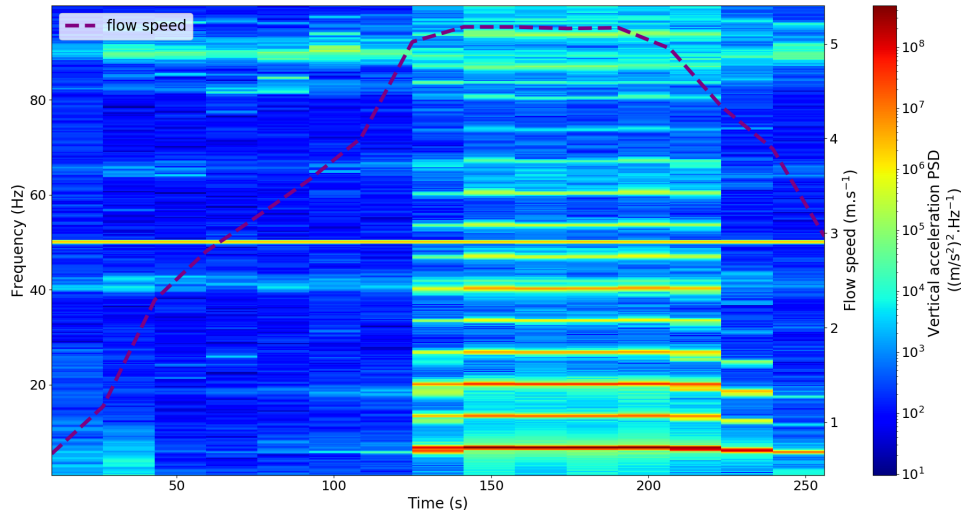

(a)

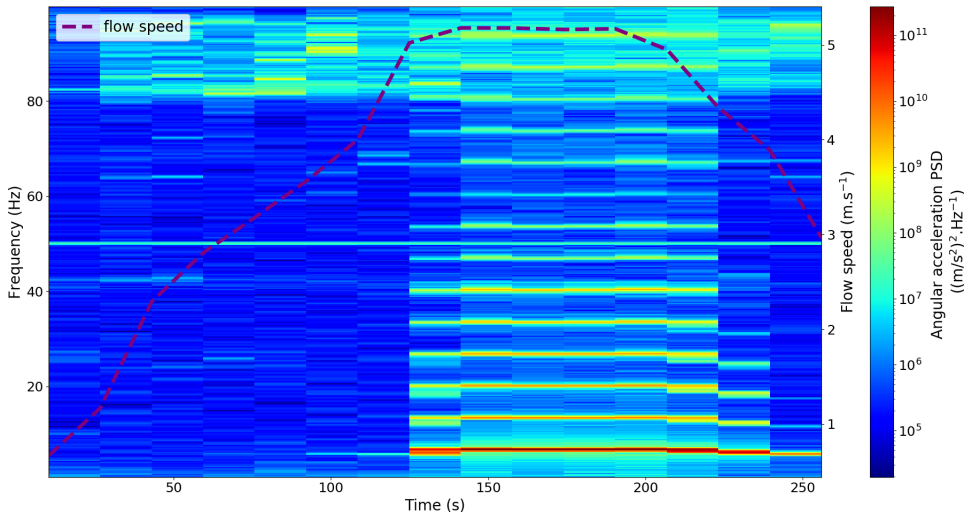

(b)

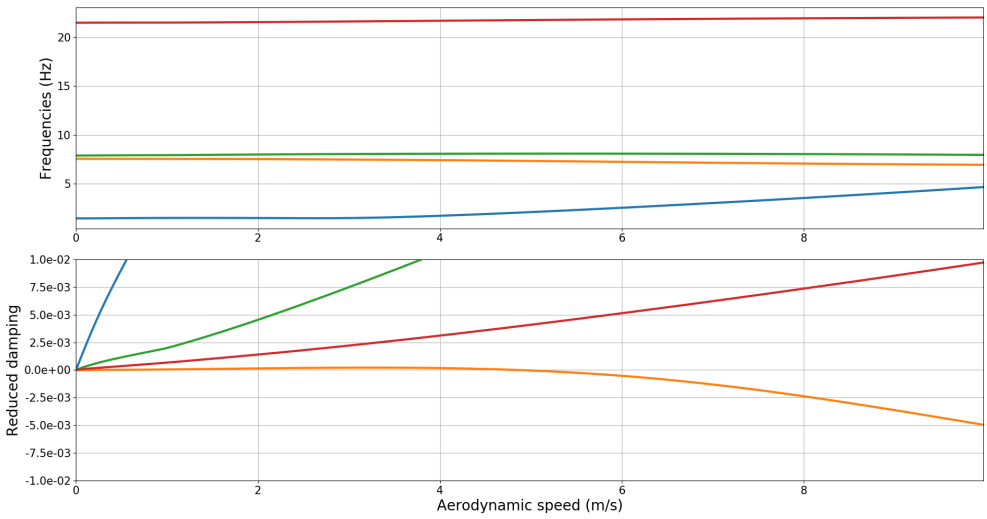

(c)

Figure 14: $420\,\mathrm{mm}$ half-span $[90, 0, 90]$ laminate test result: a) vertical acceleration spectrogram, b) angular acceleration spectrogram, c) GEBTAero aeroelastic modes plot.

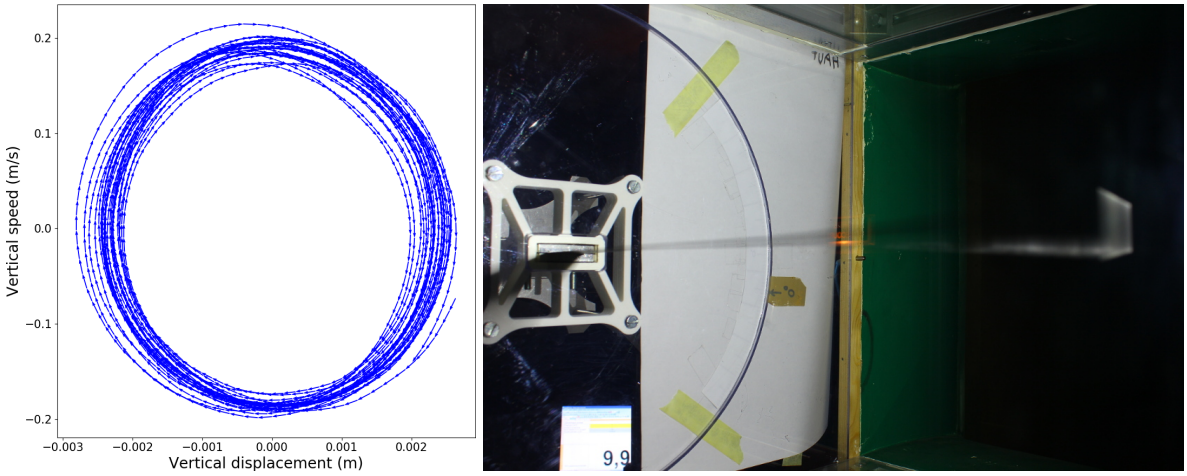

(a) (b)

Figure 15: $420\,\mathrm{mm}$ half-span flexible laminate $[15, 0, 15]$ plate LCO for a speed of $9.9\,\mathrm{m/s}$: a) verical dof phase portrait, b) long-exposure photography.

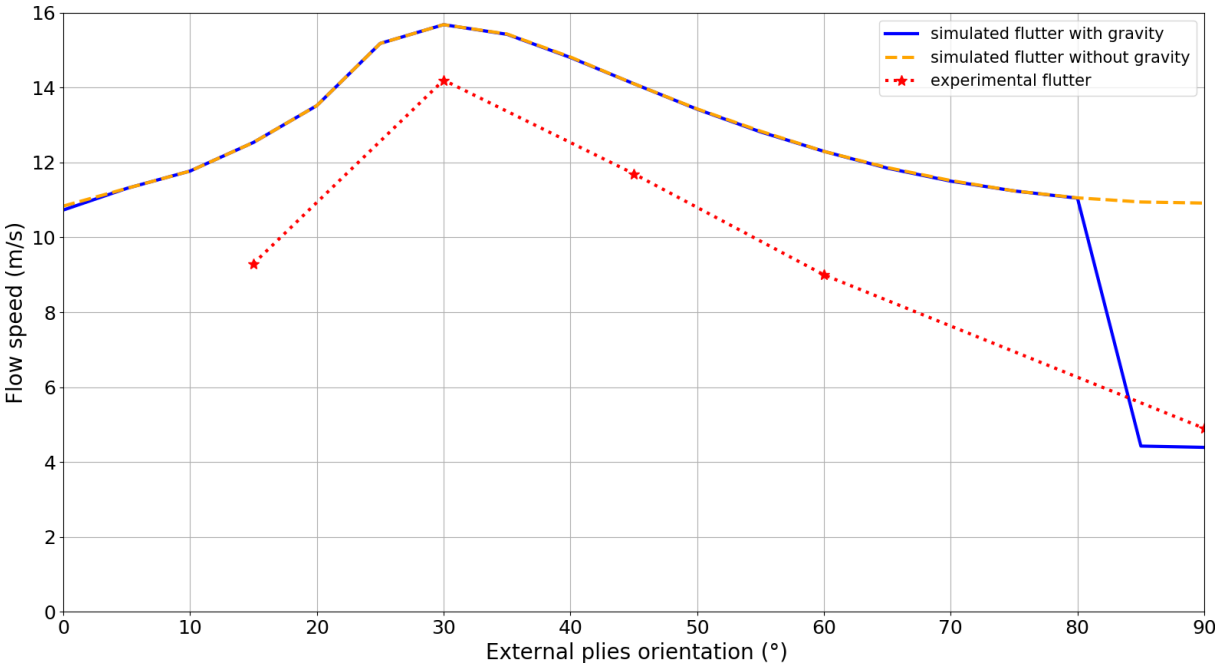

Figure 16: $420\,\mathrm{mm}$ half-span $[\theta, 0, \theta]$ laminate flutter speed with a $0°$ central ply and two variable orientation external plies θ.

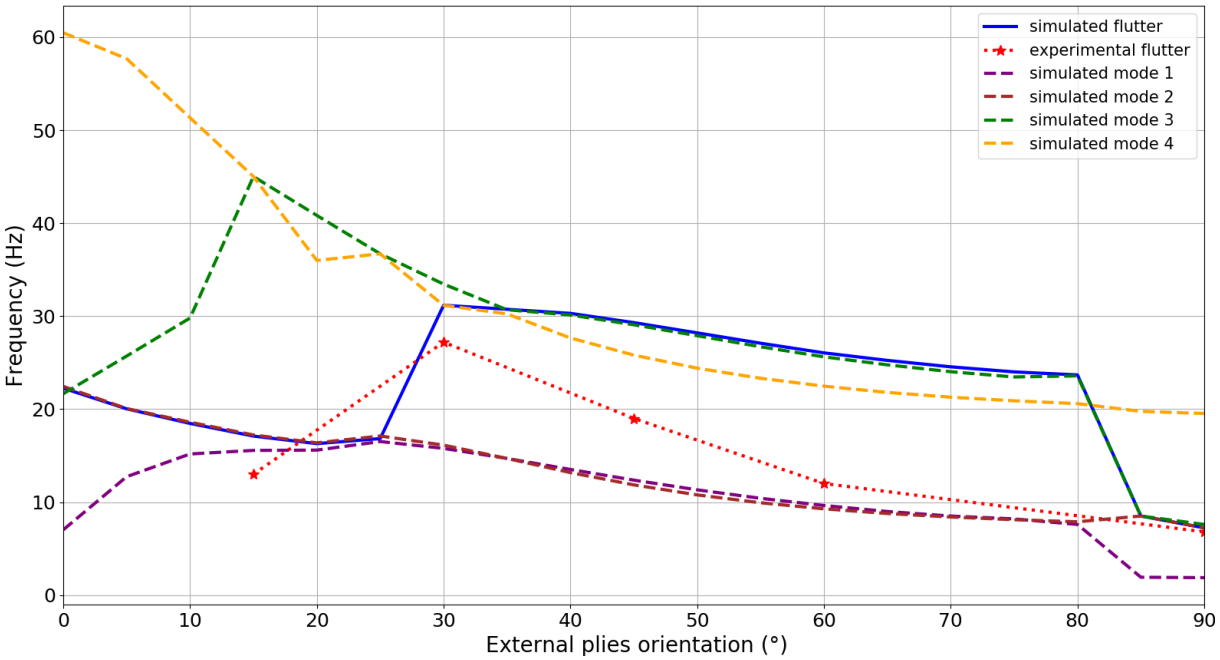

Figure 17: 420 mm half-span $[\theta, 0, \theta]$ laminate first aeroelastic modes and flutter frequencies with a $0°$ central ply and two variable orientation external plies θ.

flutter speed. $[90, 0, 90]$ laminate is the only one impacted by this static deflection. One the other hand, concerning flutter frequency, it appears that aeroelastic modes are paired on flutter boundary. Although large error can be made on simulated flutter frequency, the latter is always close to one the two mode pairs. however, the experimental flutter frequency correspond to a LCO frequency, while simulated flutter frequency correspond to the one of the unstable mode when the instability start, as provided by the harmonic analysis.

4 CONCLUSION

Design challenges induced by HAPS in terms of aeroelastic performances show the need for an accurate reduced order model able to simulate nonlinear behavior of an anisotropic high-aspect-ratio wing. The present work presents a solution based of the geometrically exact beam theory coupled with a two-dimensional unsteady finite state aerodynamic model implemented into an open source solver. Accuracy of flutter speed computation on both undeformed and deformed wing has been demonstrated using common aeroelastic test cases. In addition, to emphasis geometrical non linearities and anisotropic capabilities, a wind tunnel campaign is conducted. For the sake of simplicity, flexible metallic and composite flat plates are tested, the latter with the simplest layup exhibiting bending/twisting coupling, namely a three-ply laminate with external plies oriented in the same direction. Experimental results show a good agreement, especially for metallic plates, with two caveats. Firstly, a very slow bending mode tends to modify the static deflection of metallic plate for the highest speed, which affects the flutter speed. Secondly, the discrepancy of laminate thickness encountered during the cure process generate an uncertainties on the laminates flutter speed. Furthermore, composite plate experiments highlight the complex behaviour of such anisotropic flexible wings, with highly coupled aeroelastic modes leading to various kind of LCO.

5 REFERENCES

[1] Wang, Z., Chen, P. C., Liu, D. D., et al. (2010). Nonlinear-aerodynamics/nonlinear-structure interaction methodology for a high-altitude long-endurance wing. *Journal of*

Aircraft, 47(2), 556–566.

[2] Murua, J., Palacios, R., and Graham, J. M. R. (2012). Assessment of wake-tail interference effects on the dynamics of flexible aircraft. *AIAA Journal*, 50(7), 1575–1585.

[3] Drela, M. (1999). Integrated simulation model for preliminary aerodynamic, structural, and control-law design of aircraft. *AIAA Paper*, 99, 1394.

[4] Shearer, C. M. and Cesnik, C. E. (2007). Nonlinear flight dynamics of very flexible aircraft. *Journal of Aircraft*, 44(5), 1528–1545.

[5] Peters, D. A., Karunamoorthy, S., and Cao, W.-M. (1995). Finite state induced flow models. I-Two-dimensional thin airfoil. *Journal of Aircraft*, 32(2), 313–322.

[6] Ribeiro, F. L. C., Paglione, P., da Silva, R. G. A., et al. (2012). Aeroflex: a toolbox for studying the flight dynamics of highly flexible airplanes. In *VII Congresso Nacional de Engenharia Mecânica*. São Luís - Maranhão, Brasil.

[7] Chang, C.-S., Hodges, D. H., and Patil, M. J. (2008). Flight dynamics of highly flexible aircraft. *Journal of Aircraft*, 45(2), 538–545.

[8] Kirsch, B., Montagnier, O., Bénard, E., et al. (2018). Assessment of aeroelastic tailoring effect on high-aspect-ratio composite wing flutter speed using an open source reduced order model solver. In *18 th European Conference on Composite Materials*. Athens, Greece, pp. 24 – 28.

[9] Kirsch, B., Montagnier, O., Bénard, E., et al. Open source implementation of a tightly coupled aeroelastic reduced order model suited for aeroelastic tailoring optimisation of high aspect ratio composite wing. *Journal of Fluids and Structures*, under review.

[10] Yu, W. and Blair, M. (2012). GEBT: A general-purpose nonlinear analysis tool for composite beams. *Composite Structures*, 94, 2677–2689. ISSN 0263-8223. doi: 10.1016/j.compstruct.2012.04.007.

[11] Wang, Q., Yu, W., Sprague, M. A., et al. (2013). Geometric Nonlinear Analysis of Composite Beams Using Wiener-Milenkovic Parameters. In *Proceedings of the 54th AIAA/ASME/ASCE/AHS/ASC Structures, Structural Dynamics, and Materials Conference and Co-located Events, Boston, Massachusetts*. pp. 8–11.

[12] Goland, M. (1945). The flutter of a uniform cantilever wing. *Journal of Applied Mechanics-Transactions of the ASME*, 12(4), A197–A208.

[13] Patil, M. J. (1999). *Nonlinear aeroelastic analysis, flight dynamics, and control of a complete aircraft*. Ph.D. thesis, Citeseer.

[14] Kirsch, B., Montagnier, O., Bénard, E., et al. (2018). Computation of very flexible high-aspect-ratio composite wing flutter speed using optimised open source solver. In *53rd 3AF International Conference on Applied Aerodynamics Multiphysics approach in Aerodynamics*. Salon de Provence, France.

[15] Tang, D. and Dowell, E. (2016). Experimental aeroelastic models design and wind tunnel testing for correlation with new theory. *Aerospace*, 3(2), 12.

[16] Amestoy, P. R., Duff, I. S., L'Excellent, J.-Y., et al. (2001). A fully asynchronous multifrontal solver using distributed dynamic scheduling. *SIAM Journal on Matrix Analysis and Applications*, 23(1), 15–41.

[17] Lehoucq, R. B., Sorensen, D. C., and Yang, C. (1997). ARPACK Users' Guide: Solution of Large Scale Eigenvalue Problems with Implicitly Restarted Arnoldi Methods. *Software Environ. Tools*, 6.

[18] Hodges, D. H. (1990). A mixed variational formulation based on exact intrinsic equations for dynamics of moving beams. *International journal of solids and structures*, 26(11), 1253–1273.

[19] Cartraud, P. and Messager, T. (2006). Computational homogenization of periodic beam-like structures. *International Journal of Solids and Structures*, 43(3-4), 686–696.

[20] Dhondt, G. and Wittig, K. (1998). Calculix: a free software three-dimensional structural finite Element Program. *MTU Aero Engines GmbH, Munich, Germany*.

[21] Hodges, D. H. and Pierce, G. A. (2011). *Introduction to structural dynamics and aeroelasticity*, vol. 15. Cambridge University Press.

[22] Dowell, E. H., Clark, R., Cox, D., et al. (2004). *A modern Course in Aerelasticity*, vol. 116 of *Solid Mechanics and its applications*. Dordrecht: Kluwer academic publishers. ISBN 1-4020-2711-7.

[23] Young, W. C. and Budnyas, R. G. (2017). *Roark's formulas for stress and strain*. McGraw-Hill.

COPYRIGHT STATEMENT